Available online at www.sciencedirect.com

SciVerse ScienceDirect

Proceedings of the Combustion Institute 34 (2013) 3319–3326

Proceedings of the Combustion Institute

www.elsevier.com/locate/proci

Studies on a liquid fuel based two stage flameless combustor

V. Mahendra Reddy, Darshan Sawant, Darshan Trivedi, Sudarshan Kumar *

Combustion Research Laboratory, Department of Aerospace Engineering, Indian Institute of Technology, Mumbai 400 076, India

Available online 26 June 2012

Abstract

This paper presents the experimental and numerical results for a two stage combustor capable of achieving flameless combustion mode with 20 kW thermal input and heat release density up to 5 MW/m^3. The fuel and oxidizer are supplied at ambient conditions. The concept of high swirl flows has been adopted to achieve high internal recirculation rates, residence time and increased dilution of the fresh reactants in the primary combustion zone, resulting in flameless combustion mode. Air is injected through four tangential injection ports located near the bottom of the combustor and liquid fuel is injected through a centrally mounted pressure swirl injector. Preliminary computational analysis of the flow features shows that decrease in the exit port diameter of the primary chamber increases the recirculation rate of combustion products and helps in achieving the flameless combustion mode. Based on preliminary computational studies, a 30 mm primary chamber exit port diameter is chosen for experimental studies. Detailed experimental investigations show that flameless combustion mode was achieved with evenly distributed combustion reaction zone and uniform temperature distribution in the combustor. The CO and NO_x emissions are reduced from 350 to 11 ppm and 45 to 12 ppm respectively at an equivalence ratio of 0.92, as operation of the combustor changes from conventional to flameless combustion mode. Measurement of CO and NO_x emissions show that these emissions are reduced by an order of magnitude when operated in flameless combustion mode. The acoustic emission levels are reduced by 6–8 dB as combustion mode shifts from conventional mode to flameless combustion mode.

Keywords: Two stage combustor; Flameless combustion; Ultralow NO_x emissions; Emission reduction; Liquid fuel combustion

1. Introduction

The advent of stringent pollution norms due to environmental concerns has led to the development of various low emissions combustion techniques. NO_x is one of the major pollutants as it actively participates in ozone depletion, formation of photochemical smog and acid rains [1,2]. Therefore, it is extremely important to reduce the formation of NO_x during the combustion process itself. Suppression of thermal NO_x is a better option for NO_x control [2–5]. This has led to the development of low

* Corresponding author. Fax: +91 22 2572 2602.
E-mail address: sudar@aero.iitb.ac.in (S. Kumar).

1540-7489/$ - see front matter © 2012 The Combustion Institute. Published by Elsevier Inc. All rights reserved.
http://dx.doi.org/10.1016/j.proci.2012.06.028

NO_x emission techniques [2,4–6]. To abate the NO_x formation in various combustion systems through the dilution of fresh reactants is known as flameless or mild combustion. This technique has also been referred as colorless distributed combustion (CDC) [7,8], high temperature air combustion (HiTAC) [9] and MILD combustion [10–20] in literature. Wunning and Wunning [2] and Kumar et al. [5,6] reported that internal recirculation of combustion products results in the dilution and preheating of fresh reactants which helps in suppressing the formation of NO_x and CO emissions. The reaction zone is almost invisible and uniformly distributed throughout the volume of the combustor [4–7].

To achieve flameless combustion mode, the combustion products need to be recirculated in large quantities to ensure that the flame is blown-off from primary combustion zone [8,14,21]. The recirculated hot combustion products mix with the fresh oxidizer resulting in highly preheated and diluted reactants [21–23]. Due to ultra low emissions, the application of this technique has also been proposed to gas turbine combustors [7,24,25]. Although substantial amount of work on the flameless combustion with gaseous fuels has been reported in the literature, very little work has been reported with liquid fuels [12,26]. Most of the aircraft engines and industrial combustors are operated with liquid fuels. Therefore, it becomes imperative to understand the characteristics of flameless combustion mode with liquid fuels to reduce NO_x and CO emissions from combustion systems operating with liquid fuels. Weber et al. [12] have reported experiments with externally preheated air up to 1573 K to implement the flameless combustion mode for industrial applications with natural gas, heavy and light fuel oils and coal. Derudi and Rota [26] have focused their investigations on the sustainability of mild combustion for liquid hydrocarbons using a dual nozzle laboratory-scale burner with *n*-octane as reference fuel. In these systems, air is externally preheated and inflow of reactants and exit of products are from the same plane of the combustor [12,26]. However, in certain applications, reactants need to be supplied at ambient conditions from one end of the combustor and products are expected to leave from the other end.

The present investigations focus on the development of a flameless combustor with a typical 20 kW thermal input and a heat release density of ~5 MW/m^3 using kerosene as fuel. For gaseous fuels, the density of both oxidizer and fuel is nearly equal. Therefore, the mixing and entrainment into the fresh fuel and oxidizer is relatively easy. However, flameless combustion with liquid fuel involves many difficulties due to higher density of fuel (500–600 times higher) and very low entrainment into liquid sprays. Spray formation, droplet distribution, evaporation and mixing of fuel vapor are major difficulties. Swirl based air injection scheme is adopted because swirl flows results in high recirculation rates, improved mixing, and better flame stability limits [27–29]. Preliminary computational investigations are carried out to understand the preliminary flow features in various combustor configurations. It has been observed from the experimental study that the secondary chamber helps in improved recirculation of combustion products and complete combustion [30]. Therefore, a two stage combustor concept is proposed in this present study.

2. Experimental setup details

Figure 1 shows a schematic diagram of the experimental setup and dimensional details of a typical two-stage combustor. The combustor is

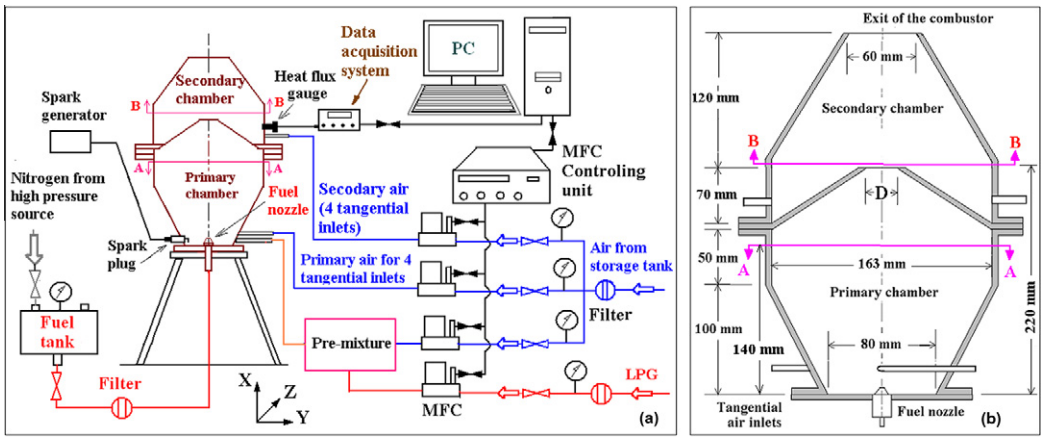

Fig. 1. (a) Schematic diagram of experimental setup and (b) detailed dimensions of the combustor.

placed vertically on a test stand as shown in the figure. Liquid fuel (kerosene) is stored in a pressurized steel tank. The fuel flow is controlled through a ball valve during the combustor operation. A pressure swirl injector with a mass flow rate of 1.72 kg/h at 9 bar injection pressure is mounted centrally at the bottom of the combustor. The spray cone angle of the injector is 45°, and the SMD at 9 bar pressure is in the range of 17–23 μm (measured with Malvern Mastersizer). The air is drawn from high pressure storage tank and controlled through electric mass-flow controllers. The combustor is initially ignited with spark-plug and run with premixed LPG–air mixture. To ensure initial flame stabilization, stoichiometric flow rates of kerosene and air are maintained. Exhaust gas composition is measured with Quintox KM-9106 gas analyzer with an O_2 analyzer (0–25% range, 0.1% accuracy), CO analyzer (0–10,000 ppm range, accuracy ±5% of reading), NO analyzer (0–5000 ppm, ±5 ppm accuracy), a C*x*H*y* analyzer (0–50,000 ppm), and a CO_2 analyzer. Continuous online measurement of the sample gas has been carried out. Temperature measurements are carried out with Omega-make KMTXL-040 (diameter = 1 mm) type thermocouple, with maximum measured temperature range of 1600 K. The measured temperature is corrected for conduction and radiation losses from thermocouple junction. Convective and radiative heat-fluxes are measured with a copper-slug type convective heat-flux gauge and radiative heat-flux gauge (Schmidt–Boelter gauge) respectively. Acoustic emissions are measured with a fast response sound level instrument (Lutron, SL-4001, $\tau_{response}$ = 200 ms) for different combustion modes. The sound level meter is placed 100 mm away from the exit plane of the combustor.

3. Evolution of the combustor geometry

The design of the combustor is based on the injection of fuel and air at ambient conditions. To achieve high recirculation rates, swirl flow configuration has been considered from the cyclone combustor systems [27–29]. Air is injected tangentially to create swirl flow. The conical shape of the combustor creates a low pressure zone at the center of the combustor. Swirl air injection creates centrifugal force that enhances the residence time of the gases trapped within the swirling flow. The increased residence time enhances the flame stability limits and recirculation of hot combustion products. The high recirculation due to swirl flow is essential for obtaining distributed reaction over a large volume of the combustor. The fuel injection through swirl injector imparts a clockwise rotation to the spray. Therefore, a counterclockwise air injection scheme is considered to impart increased shear force on the fuel spray resulting in enhanced mixing and evaporation of droplets.

3.1. Preliminary computational results

Preliminary reacting flow computational studies are carried out to understand the flow features inside the combustors of three different configurations. A general purpose CFD code Fluent-6.3 is used for solving three-dimensional Navier–Stokes equations along with energy and species conservation equations in a finite-volume domain. A number of computations were carried out using tetra-mesh which is refined after every simulation to obtain grid independent results. The number of cells was varied from 1 to 3 million. All results with ~1.5 million grid points were grid independent. Mass flow inlet condition was applied at the tangential air inlet ports. Pressure outlet boundary condition is applied at the exhaust port. Standard k–ε model is used for turbulence modeling. Kerosene ($C_{12}H_{23}$) is considered as fuel with a density of 780 kg/m^3 and a single-step based non-premixed droplet combustion model is used. A non-premixed droplet evaporation and combustion model following spherical law is considered with pre-PDF model. A solid cone type spray with a cone angle of 45° is considered with a uniform droplet diameter of 17 μm based on experimental measurements. The solution is considered to be converged when scaled residuals of the flow, species are less than 10^{-5} and energy are less than 10^{-6}.

Based on the exit diameter of the primary chamber, three different configurations are considered. The outlet diameter of the primary chamber is varied from 30 to 60 mm, with remaining dimensions same. For stoichiometric combustion, 95% of air is injected in the primary chamber and remaining 5% is injected in secondary chamber to avoid melting of air supply tubes connected to secondary chamber. For lean combustion cases, 50% of the excess air along with stoichiometric air is injected in the primary chamber. The remaining 50% of excess air is injected in the secondary chamber. The excess air injected in the secondary chamber helps in complete combustion and reduction of unburned hydrocarbons and CO emissions [30]. The variation of axial velocity for 30 mm (D30 case) exit port diameter of primary chamber is shown in Fig. 2. Significant reverse flow occurs within the primary chamber as seen from the negative magnitude of the axial velocity. The comparison of axial velocity at two different axial locations of 30 mm and 110 mm for different exit diameters is shown in Fig. 3. For all three cases, at an axial distance of 30 mm, a maximum velocity of −11.7 m/s is achieved. Whereas, at an axial location of 110 mm, the maximum velocity is −4.15, −3.8 and 1.08 m/s for 30 (D30), 45 (D45) and 60 mm (D60) exit diameters of primary cham-

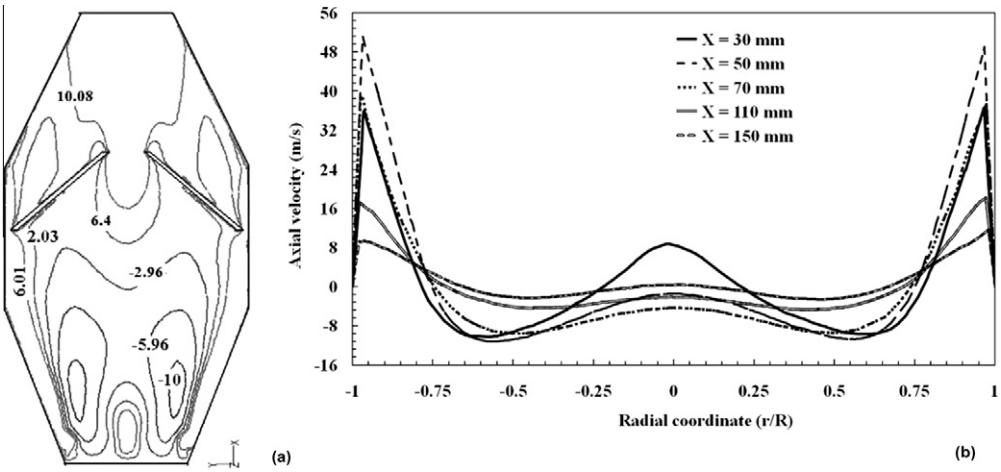

Fig. 2. Variation of the axial velocity in 30 mm primary chamber exhaust diameter combustor; (a) axial velocity contours and (b) variation of axial velocity along the radial direction.

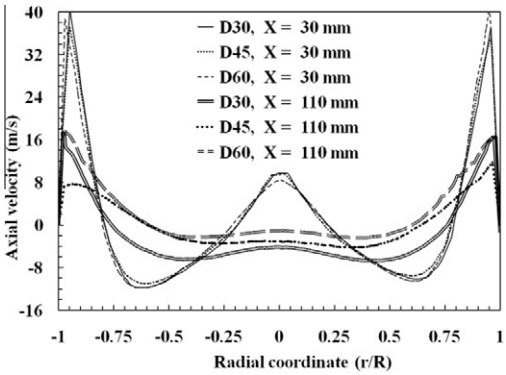

Fig. 3. Variation of the axial velocity in radial direction at two different axial locations of 30 and 110 mm for all three combustor configurations.

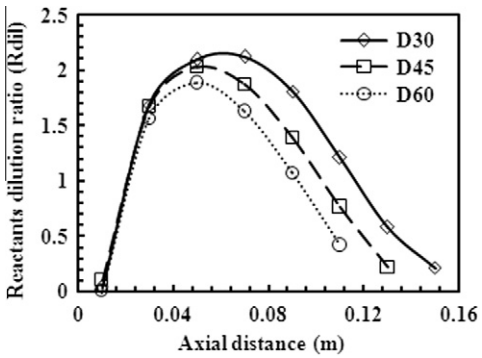

Fig. 4. Variation of reactants dilution ratio (R_{dil}) along the combustor axis for various combustors (30 mm, 45 mm and 60 mm).

ber respectively. This indicates that the length of the recirculation zone increases with a decrease in the primary chamber exit port diameter, as shown in Fig. 3. The variation of reactants dilution ratio for three combustors is shown in Fig. 4.

Reactant dilution ratio (R_{dil}) is the ratio of net mass flow rate interaction in a plane to the total mass flow rate of the reactants. It is a measure of the recirculation of the combustion products and their interaction with the fresh mixture [2,5,21]. Reactant dilution ratio is calculated as follows:

$$R_{dil} = \frac{\dot{m}_{axial} - (\dot{m}_{ox} + \dot{m}_f)}{(\dot{m}_{ox} + \dot{m}_f)}$$

$$\dot{m}_{axial} = \iint \rho v_{axial} dydz$$

Here $\dot{m}_{axial}$ is total mass flow interacting at a given plane, $\dot{m}_{ox}$ and $\dot{m}_f$ are the mass flow rates of oxidizer and fuel respectively. ρ and v_{axial} are the density and axial velocity.

Reactants dilution ratio, R_{dil} and zone length of recirculation increases with a decrease in the exit port diameter of the primary chamber because reduction in exit port size increases the reverse flow. A maximum dilution ratio of 1.89 is achieved for D60 case at an axial location of 50 mm and it reduces sharply to 0.42 at an axial length of 110 mm. For D30 case, a maximum dilution ratio of 2.19 is achieved at an axial position of 70 mm. R_{dil} greater than 2.0 exists for a zone length of ~30 mm as seen in Fig. 4. R_{dil} is greater than 1.0 for a zone length of 100, 80 and 70 mm for D30, D45 and D60 combustors respectively.

Table 1
Summary of combustion for different combustors with various air inlets.

60 (D60 case)	3, 4, 5	Big yellow flame stabilized at the center. High flow velocities causes increased shear, hence local flame extinction occurred. Hence 30 ml of fuel accumulated in the combustor.
	6	No flameless combustion and no fuel accumulation.
45 (D45 case)	3, 4	Big yellow flame stabilized at the center. High shear flow causes local flame extinction. Hence 30 ml of fuel left unburnt.
	5	Partial flameless combustion, ~10 ml fuel left unburnt
	6	Partial flameless combustion and no fuel accumulation.
30 (D30 case)	3,4	No flameless combustion. 10 ml fuel left unburnt
	5	Partial flameless combustion. Fuel droplets hitting the walls resulting in wet and cold combustor walls.
	6	Flameless combustion mode

3.2. Preliminary experimental studies

Preliminary experiments were conducted on all three combustors with a total fuel consumption of 760 ml for a duration of 21 min. Tangential velocity of air inlets has been fixed in the range of 50–70 m/s. Initially all the three combustors (D30, D45 and D60) are tested with different air inlet diameters. A brief summary of preliminary experimental observations is given in Table 1. The heat from the intermediate cone (middle plate) is helpful in improving the evaporation of liquid fuel droplets in the primary chamber as part of the spray directly strikes with it. The secondary air is injected near the intermediate cone. The combined effect of secondary air injection and fuel spray helps in maintaining the temperature of middle cone within permissible limits. The reactants dilution ratios are relatively smaller for D45 and D60 cases as compared to D30 case.

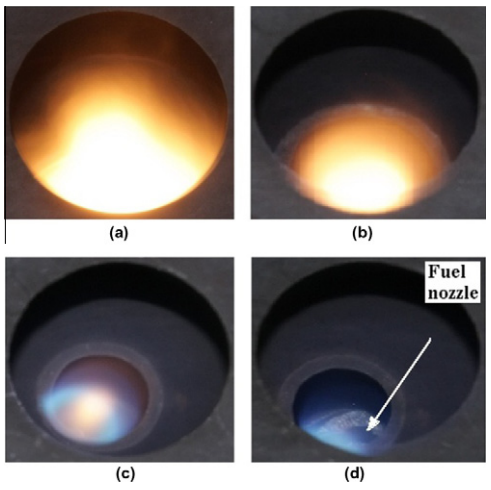

Fig. 5. Photographs of various combustion modes and transition from conventional to flameless combustion mode for different combustors, (a) 45 mm combustor, and (b–d) 30 mm combustor.

Therefore, for D60 case, a thick yellowish diffusion flame is observed along the central axis of the combustor and it is extended till the exit of the secondary chamber. Similarly, various experiments on D45 case showed that it was not possible to achieve flameless combustion mode. However, the size of yellowish diffusion flame was reduced and it became a wick-type diffusion flame. The flame was mostly stabilized in the primary chamber as shown in Fig. 5a. R_{dil} increases with a decrease in the exit port diameter of the primary chamber. The increased preheating and dilution of the fuel and oxidizer due to high R_{dil} improves the droplet evaporation rate and spreads the reaction zone uniformly throughout the combustor volume. Therefore, the conventional yellow flame gradually disappears and it transforms into flameless mode. Due to this, flameless combustion mode is achieved for D30 case. For higher inlet velocities, although the recirculation is expected to increase, higher flow velocities results in increased shear. Due to this increased shear, the flame extinction occurs in the combustor and it becomes difficult to stabilize combustion. The transition from conventional to flameless mode for D30 case is shown in Fig. 5b–d. The fuel injection nozzle on the bottom injection plane of the combustor is clearly visible as shown in Fig. 5d.

4. Results and discussion

The two stage combustors are mounted on the test stand and detailed experiments were conducted. Various measurements were carried out in the combustors as discussed below.

4.1. Temperature measurements

The radial temperature variation in the primary and secondary chamber is measured at A–A and B–B planes (see Fig. 1). The temperature distribution in primary and secondary chambers (A–A and B–B) at $\Phi = 0.92$ is shown in Fig. 6a. Since fresh oxidizer enters through tangential

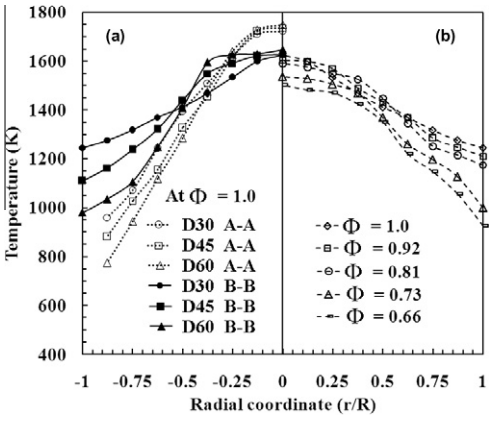

Fig. 6. Variation of temperature distribution in radial direction for all three combustors in primary and secondary chambers (a) at A–A and B–B planes ($\Phi = 1$) (b) At B–B plane of D30 combustor for different mixture equivalence ratios.

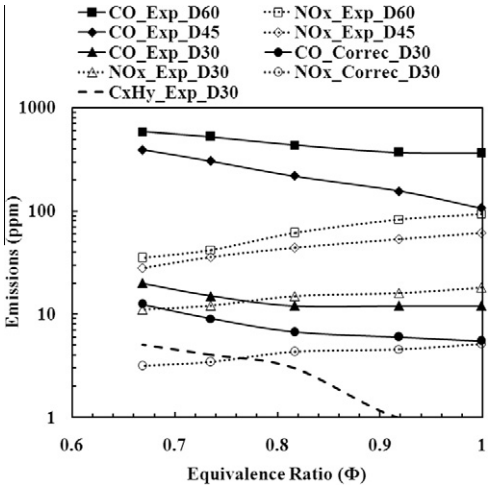

Fig. 7. Variation of emission levels at different equivalence ratios for D30, D45 and D60 combustors.

inlets and creates a very strong swirl flow, the temperature in the near wall region is relatively lower (700–900 K) for all the three combustors. Due to strong swirl flow in the near wall region, temperature variation is relatively large in primary chamber. The temperature increases towards the center of the combustor and reaches to a maximum value of 1720–1750 K for all the three combustors. At section B–B, a slightly different trend is observed. The temperature in the near wall region is in the range of 1000–1300 K and increases to 1650 K at the center. For D30 combustor, the overall temperature variation is reasonably small as compared to D45 and D60. The variation of temperature distribution with mixture equivalence ratio in the secondary chamber for D30 case is shown in Fig. 6b. The difference between the temperature at center and near-wall location decreases with an increase in the mixture equivalence ratio. It can be observed from Fig. 6b that for an equivalence ratio of 0.92 and 0.66, the difference in the near wall and center temperature is 382 K and 573 K respectively. The temperature distribution in central zone becomes more flatter with an increase in equivalence ratio.

4.2. Pollutant emissions

The variation of the composition of various combustion species such as CO, NO_x and C_xH_y (UHC) at the exit of the combustor for different equivalence ratios is shown in Fig. 7. Arghode et al. [8] have considered 15% of O_2 level in as a standard and compared the emissions from flameless combustor configurations of many researchers. Hence in the present study, the measured emissions are corrected to 15% O_2 levels for the convenience of comparison with existing literature. At $\Phi = 0.92$, measured CO and NO_x emissions for D60 combustor are 360 and 90 ppm respectively. For D30 combustor, unburned hydrocarbons emissions of 0 ppm at $\Phi = 1$ and 0.92 are observed. Since the residence time of reactants in the combustor decreases for increased flow rates (lower equivalence ratios), the concentration of C_xH_y emissions increases to 5 ppm at $\Phi = 0.66$. The experimentally measured CO emissions remain constant at 12 ppm for $\Phi = 1$ and 0.8 and increases to 20 ppm at $\Phi = 0.66$. A marginal increase in the CO emissions with a decrease in Φ can be attributed to the reduced residence time of the reactants within the combustor volume. The corrected and measured NO_X emissions vary in the range of 3–6 ppm and 11–18 ppm respectively for Φ varying from 1 to 0.66. These emissions are relatively very small as compared to a conventional combustion mode and they are of same order as that of flameless combustion with gaseous fuels [1,2,5–7,12–14,26,27]. A brief comparison of emissions from present combustor with previous work is given in Table 2. The present experimental study shows that it is possible to achieve flameless combustion mode with liquid

Table 2
Summary and comparison of emissions (ppm) normalized to 15% O_2.

Refs.	Φ	NO_x	CO	T_{air} (K)
[2]	0.9	11	-	1100
[7]	0.6	8	28	300
[12]	1.0	9	10	1600
[14]	0.8	1	10	723
[26]	1	11	3	1173
[27]	0.1	5	225	300
Present	0.92	5	6	300

fuels at high heat release densities and very low emissions of CO and NO_x.

4.3. Convective and radiative heat flux

The convective and radiative heat fluxes have been measured by inserting the heat flux gauges in the walls of combustor (Fig. 1a). It is ensured that the surface matches well with the surface of inner wall of the combustor. The gauge has been insulated from the hot wall to avoid lateral heat conduction from combustor walls. The heat flux is measured for different equivalence ratios for all three combustors as shown in Fig. 8. For D45 and D60 cases, the recirculation rate of combustion products is less, hence flame is stabilized at center of the combustor and convective heat transfer rate towards combustor walls is relatively small. For D30 case, the recirculation rate increases, thus resulting in a well distributed and uniform heat release in the combustor volume. At $\Phi = 0.92$, the convective heat fluxes of 280, 340 and 400 kW/m^2 are measured for D60, D45 and D30 combustors respectively. The radiative heat flux remains almost constant for all the cases. For D30 combustor, it is observed that for stoichiometric mixtures, the convective heat flux is ~420 kW/m^2 and it decreases to 260 kW/m^2 at an equivalence ratio of 0.66. The variation of radiative heat flux is in the range of 31–24 kW/m^2 as Φ decreases from 1 to 0.66. Overall, radiative heat flux constitutes ~7–9% of the total heat transfer in flameless combustion mode [31]. It is observed that in the case of flameless combustion mode, the heat distribution and heat transfer characteristics are relatively better as compared to the operation of the combustor in conventional combustion mode. This is perhaps due to the fact that flameless combustion occurs in a distributed manner over a large volume resulting in uniform temperature distribution and improved heat transfer characteristics.

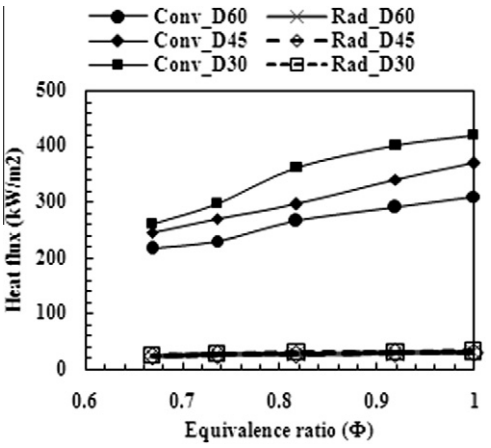

Fig. 8. Variation of convective and radiative heat flux with equivalence ratio.

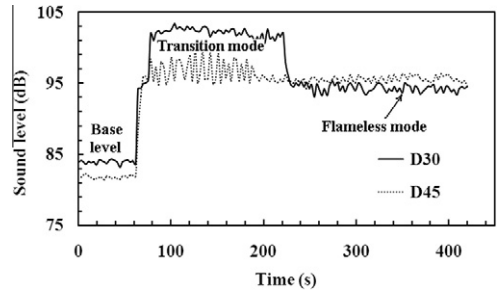

Fig. 9. Variation of acoustics emissions for D30 and D45 combustors.

4.4. Acoustic emissions

The variation of acoustic emissions during the operation of the combustors is shown in Fig. 9. The acoustic emission levels are measured at different instances of base level (non-reacting flow), transition and flameless mode with a sound level meter. For ambient conditions, a base level of 84 dB is measured at combustor outlet for D30 combustor, whereas it is slightly less for D45 combustor due to large exit diameters, thus resulting in lower noise levels. For D45 case, when the mixture is ignited, large fluctuations are observed and an average level of 97 dB is observed. For D30 case, once the combustor is ignited, the conventional flame started converting to flameless mode through transition mode and the level of acoustic emissions reaches 102 dB. As the operating mode completely shifted to flameless mode, a decrease in the acoustic emissions to 94 dB is observed. Similar reduction in the acoustic emissions has been reported by Kumar et al. [6] on a semi-industrial 150 kW combustor. Therefore, the reduction in the acoustic emissions can be attributed to the change in the operation of the combustor in flameless combustion mode.

5. Conclusions

In the present work, a new two stage combustor configuration has been shown to achieve flameless combustion with liquid fuels and air at ambient conditions. The study is an initial attempt towards the development of flameless combustion system with liquid fuel for various industrial and gas turbine applications. In future, this work will be extended to higher heat release densities. Aerothermochemical computations helped in the design of its features such as flameless combustion with reactants at ambient conditions, high heat release rates and very low CO and NO_x emissions.

The tangential air injection helps in achieving better recirculation with mixing and also gives higher residence times. The computational results show that the decrease in the port diameter of the primary chamber increases the reactants dilution ratio (R_{dil}). The maximum reactants dilution ratio of 2.19 was observed for D30 combustor. A maximum dilution ratio of 2.0 and 1.9 was observed for D45 and D 60 cases respectively. The D30 combustor is considered as an optimal combustor to achieve flameless combustion mode. Detailed experimental investigations on D30 combustor show that very low levels of emissions are formed during the flameless combustion mode. The measured CO and NO_x emissions for D60 combustor at $\Phi = 1$ are 360 and 96 ppm respectively. For D30 combustor, CO and NO_x emissions are reduced to 11 and 12 ppm respectively at $\Phi = 1$. The acoustic emission measurements show that these emissions were significantly reduced when the combustor operation shifted to flameless combustion mode from conventional combustion mode. Improved convective and radiative heat transfer characteristics were achieved for the operation in flameless combustion mode. The outstanding performance of the burner with very low chemical and acoustic emissions, high heat release rates and low combustion noise features strongly indicate the potential for use in various industrial applications.

Acknowledgements

The authors would like to acknowledge the support received for this work from 'Aeronautics Research and Development Board' (ARDB), Bangalore, India through Grant-in-Aid scheme.

References

[1] J.P. Kim, U. Schnell, G. Scheffknecht, *Combust. Sci. Technol.* 180 (4) (2008) 565–592.
[2] J.A. Wunning, J.G. Wunning, *Prog. Energy Combust. Sci.* 23 (1) (1997) 81–94.
[3] Y. Levy, V. Sherbaum, P. Arfi, *Appl. Therm. Eng.* 24 (11) (2004) 1593–1605.
[4] T. Plessing, N. Peters, J.G. Wunning, *Proc. Combust. Inst.* 27 (1988) 3197–3204.
[5] S. Kumar, P.J. Paul, H.S. Mukunda, *Proc. Combust. Inst.* 29 (2002) 1131–1137.
[6] S. Kumar, P.J. Paul, H.S. Mukunda, *Proc. Combust. Inst.* 30 (2005) 2613–2621.
[7] V.K. Arghode, A.K. Gupta, *Appl. Energy* 88 (3) (2011) 963–973.
[8] V.K. Arghode, A.K. Gupta, K.M. Bryden, *Appl. Energy* 92 (2012) 822–830.
[9] M. Katsuki, T. Hasegawa, *Proc. Combust. Inst.* 27 (1998) 3135–3146.
[10] P.R. Medwell, P.A.M. Kalt, B.B. Dally, *Combust. Sci. Technol.* 181 (7) (2009) 937–953.
[11] C. Galletti, A. Parente, L. Tognotti, *Combust. Flame* 151 (4) (2007) 649–664.
[12] R. Weber, J.P. Smart, W. Vd Kamp, *Proc. Combust. Inst.* 30 (2005) 2623–2629.
[13] M. Derudi, A. Villani, R. Rota, *Proc. Combust. Inst.* 31 (2007) 3393–3400.
[14] J. Mi, P. Li, B.B. Dally, R.A. Craig, *Energy Fuels* 23 (11) (2009) 5349–5356.
[15] M. de Joannon, A. Cavaliere, T. Faravelli, E. Ranzi, P. Sabia, A. Tregrossi, *Proc. Combust. Inst.* 30 (2005) 2605–2612.
[16] P.J. Coelho, N. Peters, *Combust. Flame* 124 (3) (2001) 503–518.
[17] A. Cavaliere, M. de Joannon, *Prog. Energy Combust. Sci.* 30 (4) (2004) 329–366.
[18] A. Parente, J.C. Sutherland, B.B. Dally, L. Tognotti, P.J. Smith, *Proc. Combust. Inst.* 33 (2011) 3333–3341.
[19] A. Parente, C. Galletti, L. Tognotti, *Proc. Combust. Inst.* 33 (2011) 3343–3350.
[20] G.G. Szegö, B.B. Dally, G.J. Nathan, *Combust. Flame* 154 (1–2) (2008) 281–295.
[21] S. Kumar, P.J. Paul, H.S. Mukunda, *Combust. Sci. Technol.* 179 (10) (2007) 2219–2253.
[22] V.M. Reddy, D. Trivedi, S. Kumar, *Combust. Sci. Technol.* 184 (1) (2012) 44–63.
[23] P.R. Medwell, P.A.M. Kalt, B.B. Dally, *Combust. Flame* 152 (1–2) (2008) 100–113.
[24] O. Lammel, H. Schütz, G. Schmitz, et al., *ASME J. Eng. Gas Turbines Power* 132 (12) (2010) 121503.
[25] R. Lückerath, M. Meier, M. Aigner, *ASME J. Eng. Gas Turbines Power* 130 (1) (2008) 011505.
[26] M. Derudi, R. Rota, *Proc. Combust. Inst.* 33 (2011) 3325–3332.
[27] R.A. Yetter, I. Glassman, H.C. Gabler, *Proc. Combust. Inst.* 28 (2000) 1265–1272.
[28] A.E.E. Khalil, A.K. Gupta, *Appl. Energy* 88 (11) (2011) 3685–3693.
[29] K.A. Al-attab, Z.A. Zainal, *Appl. Energy* 88 (4) (2011) 1084–1095.
[30] S. Hayashi, H. Yamada, M. Makida, *Proc. Combust. Inst.* 30 (2005) 2903–2911.
[31] R. Weber, F. Breussin, *Proc. Combust. Inst.* 27 (1998) 2957–2964.